Bull. Chem. Soc. Jpn., 70, 1559—1572 (1997)

Pulsed Electric Linear Dichroism of Poly(dA)·Poly(dT)·Poly(dT) and Poly(rA)·Poly(rU)·Poly(rU) in Solutions

Noriyuki Ojima, Kunihiko Gekko, and Kiwamu Yamaoka*

Department of Materials Science and Graduate Department of Gene Science, Faculty of Science, Hiroshima University, 1-3-1 Kagamiyama, Higashi-Hiroshima 739

(Received January 29, 1997)

The dependence of reduced dichroism ($\Delta\varepsilon/\varepsilon$) of sonicated rodlike title triplexes with the counterion Mg^{2+}, $(dA)_n\cdot(dT)_n\cdot(dT')_n$ and $(rA)_n\cdot(rU)_n\cdot(rU')_n$, on the wavelength (190—300 nm) and on the applied-field strength (3.8—23.1 kV cm^{-1}) was studied in aqueous ionic solutions at 7 °C. The sonicated samples were fractionated and well-characterized by the gel-permeation chromatography/low-angle laser light-scattering method. The reduced dichroism saturated at infinitely high electric fields ($(\Delta\varepsilon/\varepsilon)_s$) was estimated to be −1.22 for $(dA)_n\cdot(dT)_n\cdot(dT')_n$ and −1.09 for $(rA)_n\cdot(rU)_n\cdot(rU')_n$, by fitting the observed $\Delta\varepsilon/\varepsilon$ values at 260 nm to a theoretical orientation function. The electric linear dichroism (ELD) spectra, i.e., the dependence of $(\Delta\varepsilon/\varepsilon)_s$ on the wavelength, of $(dA)_n\cdot(dT)_n\cdot(dT')_n$ and $(rA)_n\cdot(rU)_n\cdot(rU')_n$ were determined. The measured ELD spectra were simulated by assigning the appropriate roll (θ_R) and tilt (θ_T) angles to the constituent bases. The most probable θ_R and θ_T values, determined for each triplex, indicate that the structures of triple helices both belong to an "A-form" family. The constituent bases in base-triple do not lie on a common plane. From an analysis of transient decay signals, the translation per base-triple (h) was estimated for each triplex. The structures of the present high molecular-weight triple-stranded helices in aqueous solution were determined for the first time and the plausible structural models were constructed from the experimentally evaluated sets of θ_R and θ_T.

Since Watson and Crick discovered the double-stranded helix structure of B-DNA,[1] attempts have been made to confirm diverse structures for the double and multi-stranded helices. Felsenfeld et al. first discovered the triple-helix structure of poly(rA)·poly(rU)·poly(rU) (hereafter abbreviated as $(rA)_n\cdot(rU)_n\cdot(rU')_n$, the third base or strand is specified with a prime).[2] Later, other triple helices were observed in several polynucelotide systems. Arnott and Bond determined the triple-helix structure of $(rA)_n\cdot(rU)_n\cdot(rU')_n$ for the first time by the X-ray fiber diffraction method.[3] They assigned the structure to the A′ form: the sugar puckering was in a C_3'-*endo* conformation, the bases relative to the helix axis were less inclined, and the translation per base-triple was longer than the A form. Arnott and Selsing determined the structure of poly(dA)·poly(dT)·poly(dT) (hereafter abbreviated as $(dA)_n\cdot(dT)_n\cdot(dT')_n$) in the fiber state: the structure was similar to that of $(rA)_n\cdot(rU)_n\cdot(rU')_n$, the sugar also being in C_3'-*endo* conformation.[4] Some triple-helical oligonucleotides were investigated in aqueous solutions by NMR methods;[5—9] the purine strands of triple helices were assigned to the conformation of B-form DNA with C_2'-*endo* sugar puckering.[5,8,9] Howard et al. investigated the backbone structure of $(dA)_n\cdot(dT)_n\cdot(dT')_n$ in D_2O by an infrared spectroscopic method.[10] They concluded that the conformation of the three strands of this triple helix was close to that of B-form DNA with C_2'-*endo* sugar puckering. The diverse helix structures, determined in previous studies, all depend on the molecular weight and the environment surrounding the samples; namely, high-molecular-weight polymers for X-ray measurements only in the fiber state, low-molecular-weight oligonucleotides for NMR measurements, and deuterated samples in solution for infrared measurements. The structures of high-molecular-weight triple helices have not yet been determined in aqueous solutions.

Pulsed electric linear dichroism (ELD) is an effective method for studying the solution conformation of biological polyelectrolytes with ordered chromophores. The ELD data are more accurate than those of the stretched film and flow dichroism methods, because the polymers are oriented easily and also unidirectionally by applied electric fields. A number of nucleic acids, proteins, and other related polyelectrolytes have been studied in solutions by the ELD techniques in order to clarify their higher-order structure and electric properties.[11—23] The polydispersity of the molecular weights, the overlap of the absorption bands, and the direction of the optical-transition moment in a given chromophore must be considered for an accurate determination of the overall secondary structure of synthetic polyelectrolytes.

In the present study, the reduced dichroism ($\Delta\varepsilon/\varepsilon$) of well-defined $(dA)_n\cdot(dT)_n\cdot(dT')_n$ and $(rA)_n\cdot(rU)_n\cdot(rU')_n$ samples with Mg^{2+} counterions was measured, on a comparative basis, in ionic solutions over a wide range of field strengths. The saturated reduced dichroism ($(\Delta\varepsilon/\varepsilon)_s$) was estimated by fitting the observed $\Delta\varepsilon/\varepsilon$ values to the new permanent dipole, saturable and unsaturable induced dipole moment

ELD Studies of Nucleic Acid Structure 4. Part 3 of this series is Ref. 22.

(PD-SUSID) orientation functions theoretically derived and extended to the polydisperse system in our laboratory.[24,25] From the wavelength dependence of the $(\Delta\varepsilon/\varepsilon)_s$ values, i.e., the ELD spectrum, the roll and tilt angles of the bases (θ_R and θ_T) could be calculated, $(\Delta\varepsilon/\varepsilon)_s$ giving rise to information on the arrangement of bases relative to the helix axis. From the ELD and isotropic absorption spectra of $(dA)_n\cdot(dT)_n\cdot(dT')_n$ and $(rA)_n\cdot(rU)_n\cdot(rU')_n$ triple helices, the relative arrangements of base-triples were determined. The translation per base-triple (h) of these triple helices was estimated from an analysis of the ELD decay signals. Based on the steady-state and transient ELD data, a plausible model was proposed for each triple helix structure in aqueous solutions.

Experimental

Materials. A double-stranded poly(dA)·poly(dT) sample (abbreviated as $(dA)_n\cdot(dT)_n$), lot no. 2127860031, with sedimentation coefficients ($S_{20,w}$) of 6.3 for poly(dA) and of 4.3 for poly(dT), was purchased from Pharmacia (Uppsala, Sweden). A single-stranded poly(dT) sample (abbreviated as $(dT)_n$), lot no. 56F6706, was purchased from Sigma Chemical (St. Louis, U.S.A.). Single-stranded poly(rA) (abbreviated as $(rA)_n$), lot no. 101077, with an $S_{20,w}$ value of 8.0, and poly(rU) (abbreviated as $(rU)_n$), lot no. 401055, with an $S_{20,w}$ value of 9.2, samples were purchased from Yamasa Shoyu Co. (Choshi). A triple-stranded $(dA)\cdot(dT)_n\cdot(dT')_n$ sample was prepared by mixing $(dA)_n\cdot(dT)_n$ with $(dT)_n$ at molar fraction of 0.33 in terms of adenine in a 0.2 M (1 M = 1 mol dm^{-3}) NaCl and 0.025 M phosphate buffer (at pH 7.8) solution. Similarly, a triple-strand $(rA)_n\cdot(rU)_n\cdot(rU')_n$ sample was prepared by mixing $(rA)_n$ and $(rU)_n$ at a molar ratio of adenine 1 : uracil 2 in a 0.2 M NaCl and 0.025 M phosphate buffer (at pH 6.8) solution.[26] These triple helix solutions were stored at 4 °C. The concentration of the triple helix was determined photometrically with a molar absorption coefficient (ε) of 5670 (dm^3 mol^{-1} cm^{-1}) for $(dA)_n\cdot(dT)_n\cdot(dT')_n$ and 5540 for $(rA)_n\cdot(rU)_n\cdot(rU')_n$ at 260 nm in terms of phosphorus units.[26] All other chemicals were of reagent grade.

Sonication and Fractionation. In order to lower the molecular weight of intact triple helices,[27] sonication was carried out at 0 °C with a Tomy Seiko sonicator Model UD 200 at 20 kHz. The $(dA)_n\cdot(dT)_n\cdot(dT')_n$ sample in a 0.2 M NaCl and 0.025 M phosphate buffer (at pH 7.8) solution was sonicated for 10 min with a microtip attached to the horn at a power level of 97 W. The $(rA)_n\cdot(rU)_n\cdot(rU')_n$ sample in a 0.2 M NaCl and 0.025 M phosphate buffer (at pH 6.8) solution was sonicated with a standard tip for 20 min at 200 W, according to the well-established procedure.[26,28,29] The fractionation of the sonicated $(dA)_n\cdot(dT)_n\cdot(dT')_n$ to four fractions was carried out at 20 °C with a Sephacryl S-500HR gel column by the gel permeation chromatographic method.[22,23,29] The protocol and the result of sonication and precipitational fractionation for $(rA)_n\cdot(rU)_n\cdot(rU')_n$ were described in a previous paper.[26] The melting curves of sonicated samples were measured at 260 nm (the result of $(rA)_n\cdot(rU)_n\cdot(rU')_n$ was reported in Ref. 26, and the $(dA)_n\cdot(dT)_n\cdot(dT')_n$ data were not shown here). It was confirmed that the hyperchromisity of any samples was identical before and after the sonication for each triple helix. Thus, each sonicated sample was concluded to retain the triple helix structure with no single-stranded polymer remaining in a sample solution.

GPC/LALLS. Heavy metal ions, possibly remaining in the stock triplex solution as impurities, were removed by dialysis before the GPC/LALLS (gel permeation chromatography/low angle laser light scattering) measurement, as described elsewhere in detail.[22] The stock $(dA)_n\cdot(dT)_n\cdot(dT')_n$ solution was further dialyzed against a buffer solvent containing 0.08 M NaCl, 0.0033 M $MgCl_2$, and 0.01 M Tris/HCl (ionic strength 0.1 and pH 7.8) at 7 °C for 3 d to increase the stability of $(dA)_n\cdot(dT)_n\cdot(dT')_n$ at elevated temperatures. The measurement of GPC/LALLS was carried out at 30 °C in 0.08 M NaCl, 0.0033 M $MgCl_2$, and 0.01 M Tris/HCl for $(dA)_n\cdot(dT)_n\cdot(dT')_n$ and in 0.2 M NaCl and 0.025 M phosphate buffer solution for $(rA)_n\cdot(rU)_n\cdot(rU')_n$ on a Tosoh flow-type system (the refractive index detector was operated at 35 °C), as described in previous papers.[26,28,29] A 0.5 cm^3 sample solution was injected at a flow rate of 0.6 cm^3 min^{-1}, the polymer concentration being 0.1—1.0 mg cm^{-3}. The weight-average molecular weight (M_w) and the distribution of the weight fraction (g_w) of each sample, eluted through the column, were evaluated using the signal intensities from a differential refractometer and a light-scattering photometer.[28]

UV Absorption and Circular Dichroism Spectra. Unsonicated triple-helix samples were used to measure the absorption and circular dichroism (CD) spectra in the ultraviolet (UV) wavelength region. The molar concentration of the triple helix in terms of mononucleotide units is 0.14 mM for $(dA)_n\cdot(dT)_n\cdot(dT')_n$ and 0.22 mM for $(rA)_n\cdot(rU)_n\cdot(rU')_n$. The absorption spectra were measured on a Shimadzu UV-250 spectrophotometer under a nitrogen-gas purge at 20±0.5°C with an attached temperature-control unit.[26,29] The CD measurement of a triple-helix solution was carried out at room temperature with a JASCO J-600 spectropolarimeter at the Instrument Center for Chemical Analysis, Hiroshima University.

Electric Linear Dichroism. Before ELD measurements, possible contaminants of heavy metal ions were removed from the stock solution in a manner similar to the pretreatment in the GPC/LALLS measurement. Furthermore, the counterion of each triple-helix solution was converted from Na^+ to Mg^{2+} by dialzing exhaustively against a solvent containing Mg^{2+} ions. The final ionic strength (I_s) of the dialyzed solution was adjusted to 0.0004 and 0.0012. It should be noted that the helical structure was stable below 50 °C for $(dA)_n\cdot(dT)_n\cdot(dT')_n$ and 75 °C for $(rA)_n\cdot(rU)_n\cdot(rU')_n$ at ionic strengths higher than 0.0004 with Mg^{2+} ions, as judged from their melting curves (not shown); however, the helical structure of $(dA)_n\cdot(dT)_n\cdot(dT')_n$ and $(rA)_n\cdot(rU)_n\cdot(rU')_n$ in the Na-form was unstable at room temperature and at ionic strengths lower than ca. 0.01. Therefore, all ELD measurements were carried out with these triplexes in the Mg-form. The pH of the triplex solution with the Mg^{2+} counterion was maintained at 7.8 for $(dA)_n\cdot(dT)_n\cdot(dT')_n$ and at 6.8 for $(rA)_n\cdot(rU)_n\cdot(rU')_n$ with Tris/HCl buffer. The weight-average molecular weight (M_w) and the degree of polydispersity (M_w/M_n) of sonicated fractions used for ELD measurements are given in Table 1. The ELD measurement was carried out at 7.00±0.05°C and at 260 nm over a wide electric field range (3.8 to 23.1 kV cm^{-1}) under a nitrogen-gas purge, unless otherwise stated. An ELD apparatus with a square-wave pulse generator was built in our laboratory.[13,18] ELD signals were accumulated, averaged, processed and recorded with a microcomputer to increase the signal-to-noise ratios. Four to thirty-six signals were generally accumulated in the ELD measurement, but the helix structure was stable enough against electric pulsing.

Analysis of Electric Dichroism

Steady-State Dichroism Data. The reduced dichroism is defined as $\Delta A/A = (A^E_{\parallel} - A^E_{\perp})/A$ or $\Delta\varepsilon/\varepsilon = (\varepsilon^E_{\parallel} - \varepsilon^E_{\perp})/\varepsilon$,[11] where $A^E_{\parallel}$ and $A^E_{\perp}$ are the field-on absorbances for the linearly polarized light beams parallel and perpendicular to the direction of externally applied electric field (E) respectively,

Table 1. Weight-Average Molecular Weight, M_w, Weight-Average Number of Base-Triple, $\langle bt \rangle_w$, and Degree of Polydispersity, M_w/M_n, of Fractionated $(dA)_n \cdot (dT)_n \cdot (dT')_n$ and $(rA)_n \cdot (rU)_n \cdot (rU')_n$ Samples

Triplexes	Fractions	M_w	$\langle bt \rangle_w$[a]	M_w/M_n
		10^4 g mol^{-1}		
$(dA)_n \cdot (dT)_n \cdot (dT')_n$[b]	F1	36.7	372	1.12
	F2	26.5	268	1.17
	F3	19.9	202	1.20
$(rA)_n \cdot (rU)_n \cdot (rU')_n$[c]	F2	42.3	420	1.39
	F3	29.3	291	1.43

a) $\langle bt \rangle_w$ is defined as M_w divided by the residue weight of a base-triple (987.6 g mol^{-1} for a dA·dT·dT′ and 1007.5 g mol^{-1} for an rA·rU·rU′ as the trisodium salt). b) This sample was fractionated with a GPC column. c) This sample was fractionated precipitationally with acetone as the precipitant.

A is the absorbance in the absence of the field, and $\varepsilon_{\parallel}^{E}$, $\varepsilon_{\perp}^{E}$, and ε are the corresponding molar absorption coefficients. If solute molecules are oriented by an external electric field without inducing electrochromism (no conformational transition), the following relationship should hold:[11,18]

$$3\varepsilon = \varepsilon_{\parallel}^{E} + 2\varepsilon_{\perp}^{E}. \tag{1}$$

The reduced dichroism at a wavelength of λ is expressed as:[11—13,15—23,29]

$$\frac{\Delta\varepsilon}{\varepsilon} = \left(\frac{\Delta\varepsilon}{\varepsilon}\right)_s \cdot \Phi(E) = \frac{3}{2}(3\cos^2\theta - 1) \cdot \Phi(E), \tag{2}$$

where $(\Delta\varepsilon/\varepsilon)_s$ and $\Phi(E)$ are, respectively, the saturated reduced dichroism and the orientation factor, which describes the degree of molecular orientation at E, and θ is the angle between the optical transition moment, which contributes to light absorption at λ, and the orientation axis (i.e., the helix axis). If a polymer system is polydisperse, the dependence of $\Phi(E)$ on the molecular weight must be considered in Eq. 2. $(\Delta\varepsilon/\varepsilon)_s$ is defined as $\Delta\varepsilon/\varepsilon$ at infinitely high fields, where solute molecules are oriented completely, and can be evaluated by fitting an appropriate theoretical PD-SUSID orientation function to the $\Delta\varepsilon/\varepsilon$ values observed over a wide electric field range.[15—17,19] Since the present polymer system is polydisperse, the molecular-weight distribution must be taken into account for the PD-SUSID orientation function.[24,25]

Figure 1 shows the base-triples of two triple helices and the rotational axes (x and y) adopted in the present work. The pseudodyad axis of the Watson–Crick type base-pair is taken as the tilt (x) axis when the base plane in the base-triple lies perpendicular to the helix axis (*the initial state*).[21] The roll (y) axis is orthogonal to both tilt (x) and helix (z) axes, passing through C_6 (T or U) and C_8 (A). The thin lines indicate the x and y axes, which are shifted in parallel to the third base dT′ or rU′. The roll, θ_R, and tilt, θ_T, angles are defined as the angles rotated around the y and x axes, respectively. The sign of θ_R and θ_T is taken to be positive for clockwise rotation, when viewed toward the positive direction of the roll or tilt axis, as indicated by arrows (Fig. 1a). If the optical transition

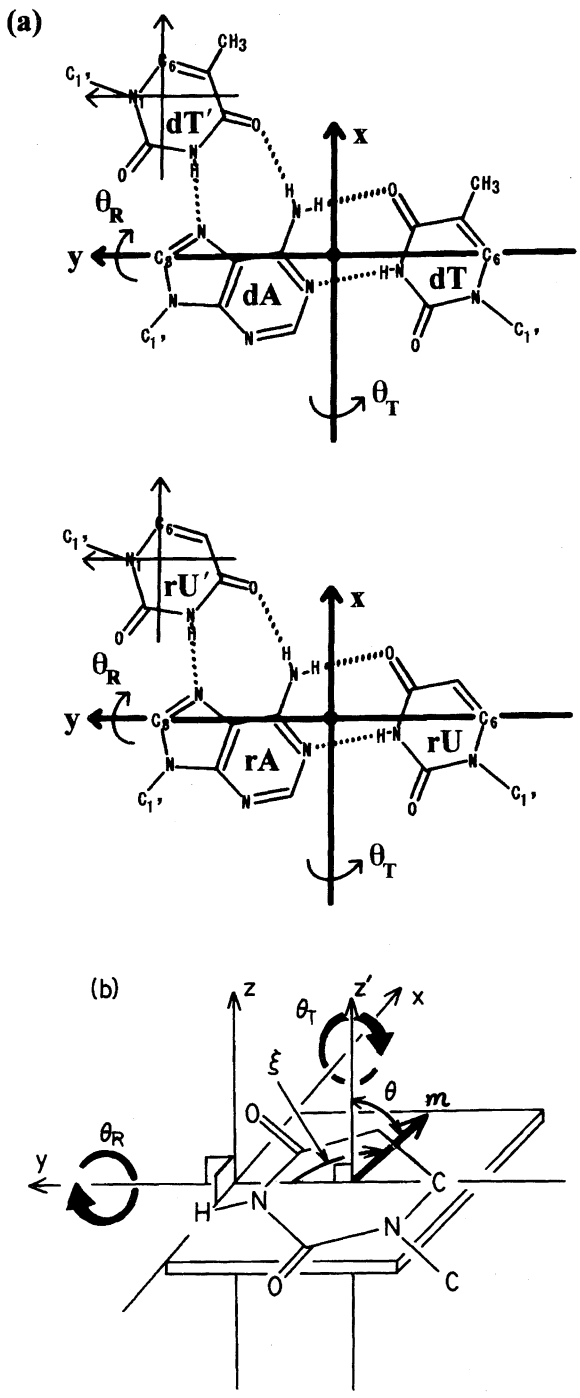

Fig. 1. Base-triples of two triplexes, the coordinate system and the definition of θ_R, θ_T, and ξ. (a) Curved arrows indicate the positive directions of rotation (c.c.w.) for the roll θ_R and tilt θ_T angles. The thin lines, passing through N_1 and C_6 atoms indicate the roll (y) and tilt (x) axes shifted parallel to the third base, respectively. dA, dT, rA, and rU strands for adenine, thymine, and uracil. dT′ and rU′ indicate the third bases. (b) The angles ξ and θ and the direction of transition moment $\boldsymbol{m}$ are defined in the framework of the Cartesian coordinate (x, y, z) system.

dipole moment ($\boldsymbol{m}$) exists on the base plane (no out-of-plane transition is considered), angle θ is related to angles θ_R and

θ_T of the base, and $(\Delta\varepsilon/\varepsilon)_s$ is rewritten as follows:[21,22,24,31]

$$\left(\frac{\Delta\varepsilon}{\varepsilon}\right)_s = \frac{3}{2}[3(-\cos\theta_T\sin\theta_R\sin\xi + \sin\theta_T\cos\xi)^2 - 1], \quad (3)$$

where ξ is the angle between $\boldsymbol{m}$ and the roll (y) axis of a given base and taken to be positive for the clockwise rotation, when viewed toward the positive direction of the z axis, as shown in Fig. 1b. The value of $\Phi(E)$ in Eq. 2 approaches unity at infinitely high electric fields for rodlike polymers; thus, $(\Delta\varepsilon/\varepsilon)_s$ at λ is given for a multicomponent absorption system as[21—23]

$$\left(\frac{\Delta\varepsilon}{\varepsilon}\right)_s = \left(\frac{3}{2}\right)\frac{\sum_j\sum_k \varepsilon_{j,k}(3\cos^2\theta_{j,k} - 1)}{\sum_j\sum_k \varepsilon_{j,k}}$$
$$= \left(\frac{3}{2}\right)\frac{\sum_j\sum_k \varepsilon_{j,k}[3(-\cos\theta_{Tk}\sin\theta_{Rk}\sin\xi_{j,k} + \sin\theta_{Tk}\cos\xi_{j,k})^2 - 1]}{\sum_j\sum_k \varepsilon_{j,k}} \quad (4)$$

where $\varepsilon_{j,k}$ is the molar absorption coefficient of the jth absorption band of the kth base. An observed ELD spectrum can be simulated by the nonlinear least-squares method, by substituting angles θ_R and θ_T to Eq. 4, and the most probable values of θ_R and θ_T may be determined for the individual base with known ξ values.[32—37] The analytical method of the ELD spectrum was described in a previous paper in detail.[21]

Values of $\varepsilon_{j,k}$ in Eq. 4 can be evaluated, by decomposing a field-absent absorption spectrum into component bands with the Gaussian band shape, as follows:[21,38]

$$\varepsilon_{j,k}(\nu) = \varepsilon_{\max,j,k}\cdot\exp\left\{-(4\ln 2)\left[\frac{\nu - \nu_{\max,j,k}}{\delta_{j,k}}\right]^2\right\}, \quad (5)$$

where $\nu_{\max,j,k}$, $\varepsilon_{\max,j,k}$, and $\delta_{j,k}$ are the peak position, the molar absorption coefficient at the peak, and the half-width of the jth band of the kth chromophore, respectively.

Electric Dichroism Decay Signals. The electric linear dichroism-average rotational relaxation time ($<\tau>_{ED}$) of a polydisperse system can be calculated from an electric dichroism decay signal after removal of the electric field. $<\tau>_{ED}$ corresponds to the area surrounded by the base line and the normalized decay curve. It can be evaluated as the sum of the three exponential curves with different decay times.[16,22] At infinitely high electric fields, $<\tau>_{ED}$ reduces to the weight-average rotational relaxation time (τ_w):[22,23]

$$\tau_w = \frac{\int \tau(M) f_w(M) dM}{\int f_w(M) dM}, \quad (6)$$

where $\tau(M)$ and $f_w(M)$ are the rotational relaxation time and the weight fraction of polymer molecules with a molecular weight of M, respectively. The value of τ_w provides information about the average length of molecules. The rotational relaxation time (τ) for a cylindrical molecule has been given by Broersma[39] as

$$\tau(L) = \left(\frac{\pi\eta_0 L^3}{18kT}\right)[\ln(L/b) - C_B]^{-1}$$

and

$$C_B = 1.57 - 7\left(\frac{1}{\ln(L/b)} - 0.28\right)^2, \quad (7)$$

where η_0 is the viscosity of the solvent, k is the Boltzmann constant, and T is the absolute temperature. L and b are the length and the radius of the cylindrical molecule, respectively. If the axial translation per base-triple and the molecular weight of the base-triple are expressed with h and M_r (987.6 for dA·dT·dT′ and 1007.5 for rA·rU·rU′), respectively, $\tau(M)$ may be calculated by substituting $h\times(M/M_r)$ to L in Eq. 7:

$$\tau(M) = \frac{\pi\eta_0 h^3 (M/M_r)^3}{18kT}\left[\ln\left(\frac{h(M/M_r)}{b}\right) - C_B\right]^{-1} \quad (8)$$

The τ_w value is iteratively calculated so as to agree with the observed value, by substituting the $f_w(M)$ and M values experimentally evaluated from the GPC/LALLS determination and an appropriate trial h value in Eqs. 6 and 8.

Results and Discussion

Weight-Average Molecular Weight and Molecular Weight Distribution. Figure 2 shows the GPC/LALLS-

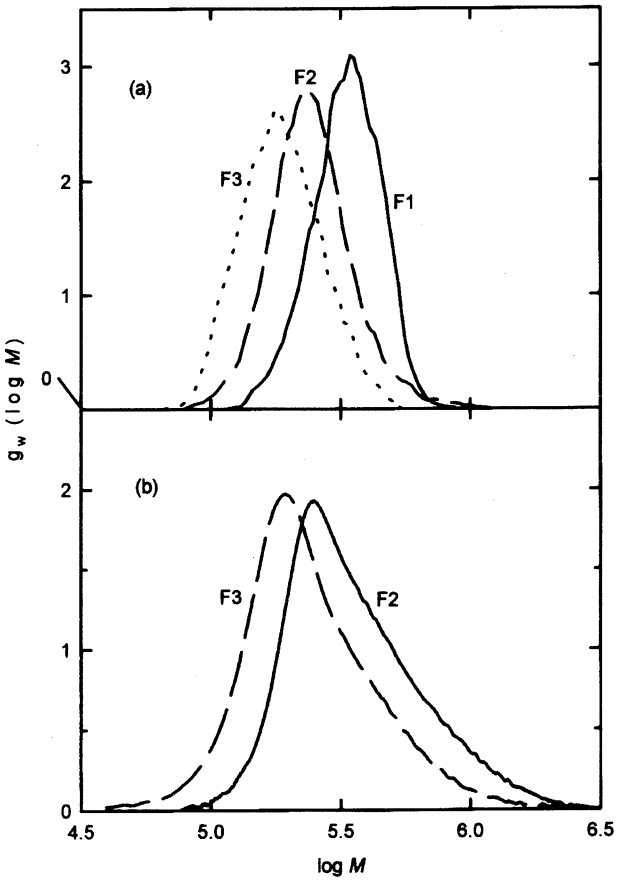

Fig. 2. GPC/LALLS-determined molecular weight distributions of $(dA)_n\cdot(dT)_n\cdot(dT')_n$ (a) and $(rA)_n\cdot(rU)_n\cdot(rU')_n$ (b) in terms of weight fraction $g_w(\log M)$ vs. molecular weight M on a semilogarithmic scale. Numerals denote the successively-fractionated samples (cf. Table 1). The area of a $g_w(\log M)$ vs. $\log M$ curve of each fraction is normalized to unity.

determined molecular-weight distributions of two sonicated and subsequently fractionated samples of $(dA)_n\cdot(dT)_n\cdot(dT')_n$ (a) and $(rA)_n\cdot(rU)_n\cdot(rU')_n$ (b) in terms of the weight fraction g_w ($\log M$) vs. molecular weight M[26,28,29] on a semilogarithmic scale. The area surrounded by the distribution curve and the abscissa was normalized to unity for each fraction. The distribution profiles shift progressively toward the lower molecular-weight side, though the curves overlap one another to some extent. The weight-average molecular weight (M_w) and the degree of polydispersity, expressed by the ratio of weight- to number-average molecular weights (M_w/M_n) of each fraction are given in Table 1. These M_w and M_w/M_n values reveal that the sonication and gel permeation chromatography techniques make it possible to prepare, in a large quantity for physicochemical studies, small-size and narrowly distributed fragments for the triple helix polynucleotides in the same manner as for the double helix polynucleotides.[28]

CD and UV Spectra. Figure 3 shows the CD (a) and UV absorption (b) spectra of $(dA)_n\cdot(dT)_n\cdot(dT')_n$ and $(rA)_n\cdot(rU)_n\cdot(rU')_n$. The CD spectra in the present study are consistent with the B-type behavior for $(dA)_n\cdot(dT)_n\cdot(dT')_n$ and A-type for $(rA)_n\cdot(rU)_n\cdot(rU')_n$, being in good agreement with those reported in previous studies.[6,10,40] Although the UV absorption spectra differ only slightly, the CD profiles show a large difference between $(dA)_n\cdot(dT)_n\cdot(dT')_n$ and $(rA)_n\cdot(rU)_n\cdot(rU')_n$, which has led to the notion that the helix conformation can possibly be different between these triple helices.[41] This difference, however, is only qualitative and mostly empirical; no quantitative discussion can be advanced from these observed UV and CD spectra, until detailed structural information is available on $(dA)_n\cdot(dT)_n\cdot(dT')_n$ and $(rA)_n\cdot(rU)_n\cdot(rU')_n$ by the ELD method.

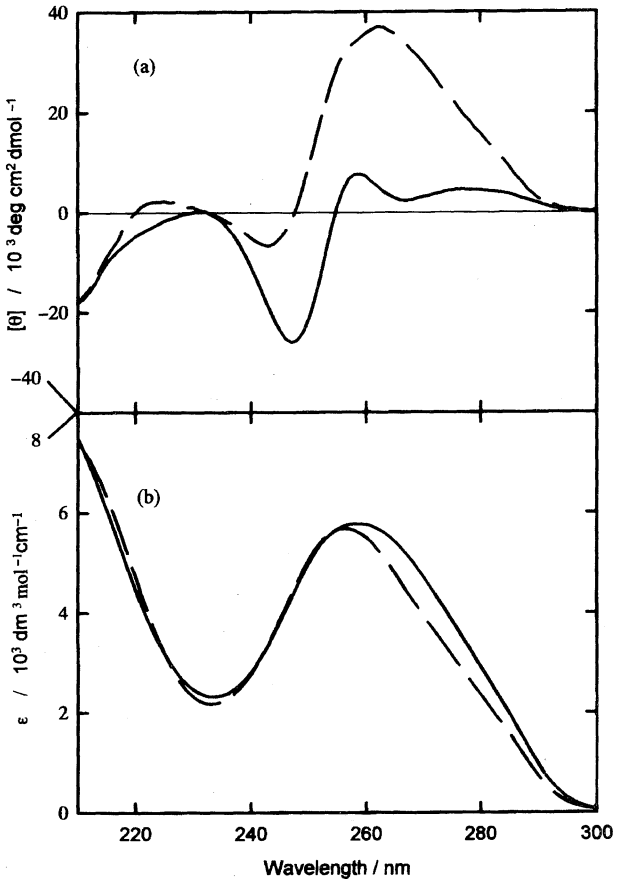

Fig. 3. CD (a) and UV absorption (b) spectra of $(dA)_n\cdot(dT)_n\cdot(dT')_n$ (solid lines) and $(rA)_n\cdot(rU)_n\cdot(rU')_n$ (broken lines) at room temperature in 0.2 M NaCl–0.025 M phosphate buffer solution. Both spectra were measured at the molar concentration of triple helix in terms of mononucleotide units: 0.14 mM for $(dA)_n\cdot(dT)_n\cdot(dT')_n$ and 0.22 mM for $(rA)_n\cdot(rU)_n\cdot(rU')_n$. The ordinates are expressed in terms of the molar ellipticity [θ] and the molar absorption coefficient ε.

Dependence of Electric Linear Dichroism on Field Strength. The saturated reduced dichroism ($(\Delta\varepsilon/\varepsilon)_s$)

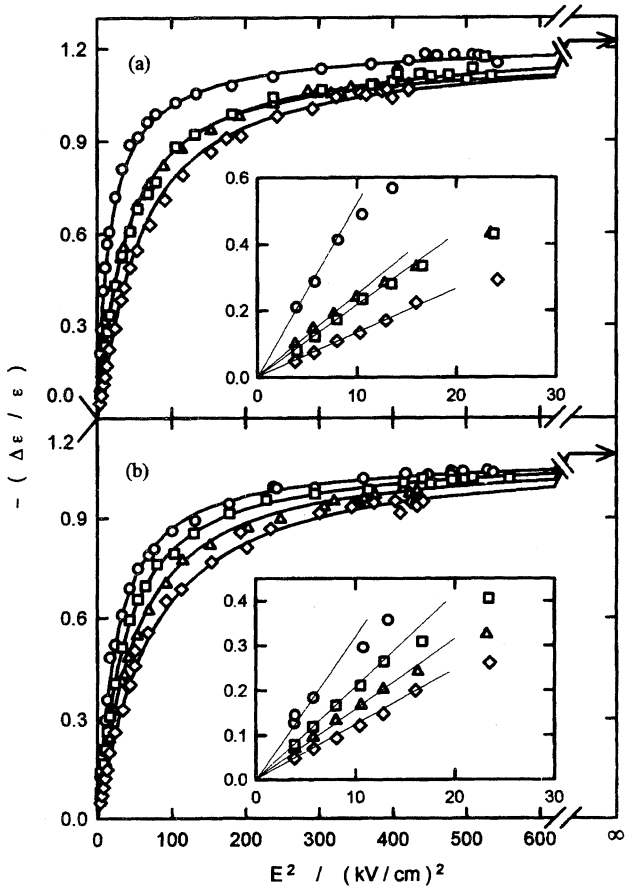

Fig. 4. Dependence of reduced dichroism $\Delta\varepsilon/\varepsilon$ of $(dA)_n\cdot(dT)_n\cdot(dT')_n$ (a) and $(rA)_n\cdot(rU)_n\cdot(rU')_n$ (b) on electric field strength in aqueous solutions with Mg^{2+}-counterion at 260 nm. Solid lines are PD-SUSID theoretical curves best-fitted to the experimental data. Arrows to the right ordinate denote the reduced dichroism values extrapolated to infinitely high fields. (a): I_s=0.0004 (F1 (○) and F3 (□)) and I_s=0.0012 (F1 (△) and F3 (◇)). (b): I_s=0.0004 (F2 (○) and F3 (□)) and I_s=0.0012 (F2 (△) and F3 (◇)). Inserts: field strength dependence of reduced dichroism in the low-field region on an expanded scale. Solid lines were drawn by the least-squares method.

Table 2. Saturated Reduced Dichroism, $(\Delta\varepsilon/\varepsilon)_s$, and Weight-Average Electric Parameters, $\Delta\alpha$, $\Delta\sigma$, E_0, and μ, of $(dA)_n\cdot(dT)_n\cdot(dT')_n$ and $(rA)_n\cdot(rU)_n\cdot(rU')_n$ in Ionic Solution with the Mg^{2+} Counterion at 7 °C

Triplexes and fractions	I_s[a] / 10^{-3}	$(\Delta\varepsilon/\varepsilon)_s$[b]	$\langle\Delta\alpha\rangle_w$ / 10^{-32} F m^2	$\langle\Delta\sigma\rangle_w$ / 10^{-31} F m^2	$\langle E_0\rangle_w$ / kV cm^1	$\langle\Delta\sigma\rangle_w\langle E_0\rangle_w$[c] / D	$\langle\mu\rangle_w$ / D
$(dA)_n\cdot(dT)_n\cdot(dT')_n$							
F1	0.4	−1.22	4.07	2.44	1.26	9220	1190
	1.2	−1.18	2.71	0.81	2.18	5290	970
F2	0.4	−1.22	2.66	1.30	2.44	9510	950
	1.2	−1.22	1.85	0.55	3.74	6170	800
F3	0.4	−1.24	1.48	0.74	3.24	7190	720
	1.2	−1.22	1.36	0.41	4.35	5350	690
$(rA)_n\cdot(rU)_n\cdot(rU')_n$							
F2	0.4	−1.09	7.67	0.77	2.24	5170	1630
	1.2	−1.08	6.81	0.07	7.53	1580	1540
F3	0.4	−1.10	3.93	0.59	3.62	6400	1170
	1.2	−1.09	3.42	0.17	6.73	3430	1090

a) I_s is the total ionic strength of the solution. b) These values were determined at 260 nm. c) This quantity is close, but not equal, to the weight-average ionic induced dipole moment $\langle\Delta\sigma E_0\rangle_w$.[24,25,42] 1 D=3.335×10^{-30} C m.

is one of the most important quantities for determining the secondary structure of nucleic acids in solution. In order to determine the orientation factor ($\Phi(E_a)$) of a triplex system at a given field strength (E_a) the dependence of the electric dichroism on the electric-field strength should be known at a fixed wavelength. Although the measurement of $\Delta\varepsilon/\varepsilon$ must be extended to infinitely high electric fields to evaluate $(\Delta\varepsilon/\varepsilon)_s$, this is an experimentally impossible task. Figure 4 shows the dependence of $\Delta\varepsilon/\varepsilon$ on the electric-field strength for $(dA)_n\cdot(dT)_n\cdot(dT')_n$ (a) and $(rA)_n\cdot(rU)_n\cdot(rU')_n$ (b). The solid lines represent the PD-SUSID theoretical orientation functions best fitted to the experimental $\Delta\varepsilon/\varepsilon$ data. It should be noted here that these functions were modified so as to take into account the molecular-weight distribution of $(dA)_n\cdot(dT)_n\cdot(dT')_n$ and $(rA)_n\cdot(rU)_n\cdot(rU')_n$.[24,25] For both triple helices, the specific parallel dichroism ($-(\Delta\varepsilon_{\parallel}/\varepsilon)$) and the specific perpendicular dichroism multiplied by a factor of 2 ($2(\Delta\varepsilon_{\perp}/\varepsilon)$) were practically superimposable on each other over an electric-field range between 3.8 and 23.1 kV cm^{-1} (not shown); hence, the relationship (Eq. 1) should hold over this electric field range with no electrochromism.[11,18] This result confirms that the secondary structure of $(dA)_n\cdot(dT)_n\cdot(dT')_n$ and $(rA)_n\cdot(rU)_n\cdot(rU')_n$ remains unaltered at high field strengths upto 23.1 kV cm^{-1}. In the low-field region, the observed $\Delta\varepsilon/\varepsilon$ values show the E^2 dependence (thin lines in Inserts); thus, the Kerr law is obeyed. The field orientation behavior of these triplexes must be quite normal, contrary to a very high-molecular-weight DNA.[15,17]

Saturated Reduced Dichroism and Electric Properties. The orientation factor ($\Phi(E_a)$) at E_a is given from the fitting of a theoretical orientation function to experimental $\Delta\varepsilon/\varepsilon$ values at a wavelength. Once this quantity is available, $(\Delta\varepsilon/\varepsilon)_s$ at any wavelength can be evaluated from the expression $\Delta\varepsilon/\varepsilon=(\Delta\varepsilon/\varepsilon)_s\cdot\Phi(E_a)$. Table 2 gives the $(\Delta\varepsilon/\varepsilon)_s$ values estimated by the curve-fitting method. These $(\Delta\varepsilon/\varepsilon)_s$ values are nearly constant, being independent of I_s and M_w: $(\Delta\varepsilon/\varepsilon)_s=-1.22\pm0.02$ for $(dA)_n\cdot(dT)_n\cdot(dT')_n$ and -1.09 ± 0.01 for $(rA)_n\cdot(rU)_n\cdot(rU')_n$ at 260 nm. The constancy of $(\Delta\varepsilon/\varepsilon)_s$ reveals that the structure of these triple helices is not affected by I_s and M_w under the present conditions. The values of angle θ at 260 nm between the transition moment direction and the helix axis were calculated from Eq. 3 to be 75.6° for $(dA)_n\cdot(dT)_n\cdot(dT')_n$ and 72.4° for $(rA)_n\cdot(rU)_n\cdot(rU')_n$. From these values, it is clear that the base planes of these triple helices are not normal to the helix axis and, hence, the helix structure probably belongs to the so-called "A-family",[41] and that the plane of a base or a base-triple of rA·rU·rU′ is more inclined than that of dA·dT·dT′ with respect to the helix axis. The difference of θ by 3.2° may be due to the chemical structure of bases and the conformation of sugars. The more specific helical structure must be unraveled from an analysis of the dependence of $(\Delta\varepsilon/\varepsilon)_s$ on the wavelength, as discussed in detail in the following sections.

The electrical properties of $(dA)_n\cdot(dT)_n\cdot(dT')_n$ and $(rA)_n\cdot(rU)_n\cdot(rU')_n$ can be evaluated from the theoretical PD-SUSID curves, which were best fitted to the experimental data. Table 2 gives the weight-average quantities of unsaturable induced electric polarizability anisotropy $\langle\Delta\alpha\rangle_w$, the saturable induced electric polarizability anisotropy $\langle\Delta\sigma\rangle_w$, the critical electric field $\langle E_0\rangle_w$, and the permanent dipole moment $\langle\mu\rangle_w$.[24,25] The ionic polarizability anisotropy is more dominant for the electric orientation of the present triple helices than the permanent dipole moment, because the values of $\langle\Delta\sigma\rangle_w\langle E_0\rangle_w$ were much larger than $\langle\mu\rangle_w$ in all cases. It should be noted from these results that the triple helices have finite values of $\langle\mu\rangle_w$ due to the directionality of the third strand in contrast with the antiparallel double-stranded helices.[22,23,42] The dependence of $\langle\Delta\sigma\rangle_w$ on I_s is larger for the

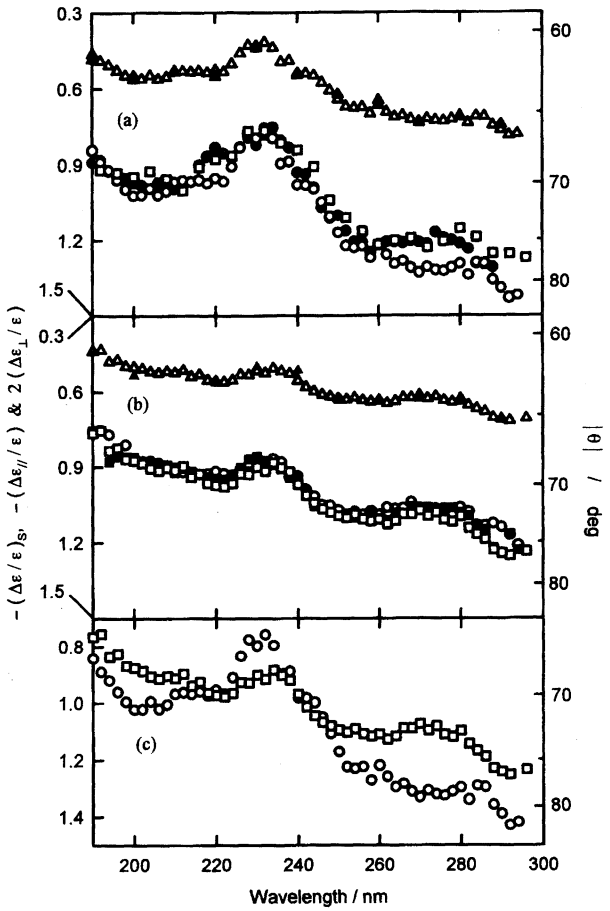

Fig. 5. Wavelength dependence of the specific parallel, $\Delta\varepsilon_{\parallel}/\varepsilon$, and specific perpendicular dichroism, $\Delta\varepsilon_{\perp}/\varepsilon$, and the saturated reduced dichroism, $(\Delta\varepsilon/\varepsilon)_s$, of $(dA)_n\cdot(dT)_n\cdot(dT')_n$ (a), $(rA)_n\cdot(rU)_n\cdot(rU')_n$ (b), and $(dA)_n\cdot(dT)_n\cdot(dT')_n$ and $(rA)_n\cdot(rU)_n\cdot(rU')_n$ (c) all in the Mg^{2+}-containing aqueous solutions. (a): $-(\Delta\varepsilon_{\parallel}/\varepsilon)$ (△) and $2(\Delta\varepsilon_{\perp}/\varepsilon)$ (▲) for F2 measured at 11.6 kV cm^{-1} and I_s=0.0004; $-(\Delta\varepsilon/\varepsilon)_s$ for F2 (○) at I_s=0.0004 and (●) at I_s=0.0012 and for F3 (□) at I_s=0.0004. (b): $-(\Delta\varepsilon_{\parallel}/\varepsilon)$ (△) and $2(\Delta\varepsilon_{\perp}/\varepsilon)$ (▲) for F3 measured at 15.3 kV cm^{-1} and I_s=0.0004; $-(\Delta\varepsilon/\varepsilon)_s$ for F2 (○) at I_s=0.0004 and for F3 (□) at I_s=0.0004, and (■) at I_s=0.0012. (c): $-(\Delta\varepsilon/\varepsilon)_s$ for F2 (○) of $(dA)_n\cdot(dT)_n\cdot(dT')_n$ and for F3 (□) of $(rA)_n\cdot(rU)_n\cdot(rU')_n$ at I_s=0.0004.

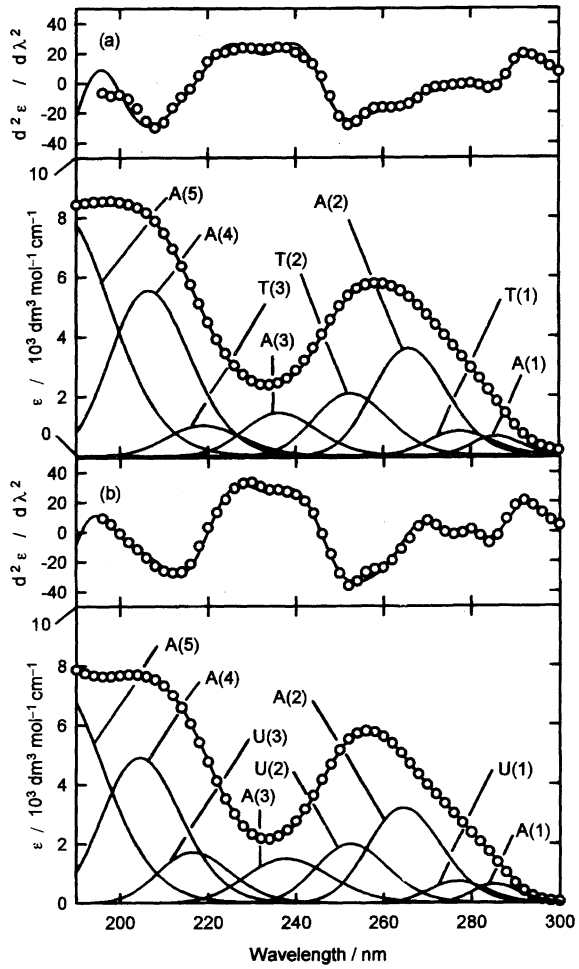

Fig. 6. Deconvolution of the isotropic absorption (bottom) and second-derivative (top) spectra for $(dA)_n\cdot(dT)_n\cdot(dT')_n$ (F2 at I_s=0.0004) (a) and $(rA)_n\cdot(rU)_n\cdot(rU')_n$ (F2 at I_s=0.0004) (b). Open circles are the experimental data, and solid lines are the individual component bands and also the sum of deconvoluted component bands. The component bands were assigned to adenine, thymine, and uracil bases with A, T, and U, respectively. T indicates both dT and dT′ bases, while U denotes rU and rU′ (cf. Table 3). Numerals in parentheses indicate the band number given in Table 3.

triple helix than for the double helix, indicating that the difference in the electrical-charge densities between triple- and double-stranded helices affects the behavior of condensed ions around the polynucleotides under an applied electric field. Although it would be very interesting to discuss these electrical properties for understanding the behavior of counterions on the surface of the triple-stranded helix and the field orientation mechanism,[43] this subject is beyond the scope of the present work.

Wavelength Dependence of Electric Linear Dichroism. Figure 5 shows the wavelength dependence of $(\Delta\varepsilon/\varepsilon)_s$, i.e., the ELD spectrum, $-(\Delta\varepsilon_{\parallel}/\varepsilon)$, and $2(\Delta\varepsilon_{\perp}/\varepsilon)$ for $(dA)_n\cdot(dT)_n\cdot(dT')_n$ (a) and $(rA)_n\cdot(rU)_n\cdot(rU')_n$ (b). $(\Delta\varepsilon/\varepsilon)_s$ at a given wavelength, λ, was calculated from $\Delta\varepsilon/\varepsilon$ at λ and the orientation factor $\Phi(E_a)$ at a fixed field strength of E_a, estimated from Fig. 4 (cf. Eq. 2). Figure 5c compares two ELD spectra of $(dA)_n\cdot(dT)_n\cdot(dT')_n$ and $(rA)_n\cdot(rU)_n\cdot(rU')_n$, which were measured under the close conditions. For these triple helices, the values of $-(\Delta\varepsilon_{\parallel}/\varepsilon)$ and $2(\Delta\varepsilon_{\perp}/\varepsilon)$ are practically equal to each other over the entire wavelength region (Figs. 5a and 5b). This result supports the notion that the helix structures are unaltered at any wavelengths under applied electric fields. The profiles of all ELD spectra of triple helices are not constant, but undulatory. The ELD spectrum of $(dA)_n\cdot(dT)_n\cdot(dT')_n$ depends slightly on I_s, but not on M_w (Fig. 5a), revealing that the helix structure is affected by counterions. These results happen to conflict with the accidental constancy of the $(\Delta\varepsilon/\varepsilon)_s$ of $(dA)_n\cdot(dT)_n\cdot(dT')_n$ at a single wavelength of 260 nm, as estimated from the dependence of $\Delta\varepsilon/\varepsilon$ on the electric-field strength in Fig. 4. There-

Table 3. Optical Characteristics and Directions of Component Bands and the assignment to Constituent Bases in $(dA)_n\cdot(dT)_n\cdot(dT')_n$ and $(rA)_n\cdot(rU)_n\cdot(rU')_n$

Triplexes		$\lambda_{maxj,k}$	$\varepsilon_{maxj,k}$	$\delta_{j,k}$	$\xi_{j,k}$/deg[a]			
Bases	Bands[b]	nm	$10^3\ M^{-1}\ cm^{-1}$	$10^3\ cm^{-1}$	*1*	*2*	*3*	*4*
$(dA)_n\cdot(dT)_n\cdot(dT')_n$								
dA	1	286	0.65	1.60	75[c]	94[d]	148[e]	75[c]
	2	266	3.60	2.80	203[c]	116[d]	58[e]	116[d]
	3	236	1.45	3.50	118[c]	32[d]	132[e]	32[d]
	4	206	5.55	5.00	118[c]	185[f]	34[e]	118[c]
	5	187	8.10	7.00	223[c]	185[f]	34[e]	223[c]
dT	1	277	0.83	2.20	65[g]	75[f]	67[e]	65[g]
	2	252	2.10	3.10	57*	87[d]	67[e]	87[d]
	3	219	1.03	4.20	−13[h]	−15[f]	47[e]	−13[h]
dT′	1	277	0.83	2.10	201[g]	191[f]	199[e]	201[g]
	2	252	2.10	3.10	219*	179[d]	199[e]	179[d]
	3	219	1.03	4.20	279[h]	281[f]	213[e]	279[h]
$(rA)_n\cdot(rU)_n\cdot(rU')_n$								
rA	1	285	6.33	1.50	75[c]	94[d]	148[e]	75[c]
	2	265	3.20	2.80	203[c]	116[d]	58[e]	116[d]
	3	238	1.50	4.00	118[c]	32[d]	132[e]	32[d]
	4	205	4.90	5.00	118[c]	185[f]	34[e]	118[c]
	5	185	7.50	7.00	223[c]	185[f]	34[e]	223[c]
rU	1	277	0.73	2.00	65[g]	75[f]	67[e]	65[g]
	2	252	2.00	3.00	47*	67[d]	67[e]	67[d]
	3	217	1.72	4.10	−3[g]	−15[f]	47[e]	−3[g]
rU′	1	277	0.73	2.00	201[g]	191[f]	199[e]	201[g]
	2	252	2.00	3.00	219*	199[d]	199[e]	199[d]
	3	217	1.72	4.10	269[g]	281[f]	213[e]	269[g]

a) Letters c–h denote references, from which ξ values were taken: c) Ref. 32; d) Ref. 35; e) Ref. 36; f) Ref. 34; g) Ref. 33; h) Ref. 31. Asterisk (*) is the angle for T(2) or U(2), which is assumed to be symmetric to that for T(1) and U(1) with respect to the reference axis of dT and rU. b) Numerals correspond to the numbered component bands in Fig. 6.

Table 4. Angles θ_R and θ_T in Degrees for Bases Obtained from the Analysis of Observed ELD Spectra of $(dA)_n\cdot(dT)_n\cdot(dT')_n$ and $(rA)_n\cdot(rU)_n\cdot(rU')_n$

Triplexes	α_k[a]				θ_{Rk}				θ_{Tk}			
bases	deg				deg				deg			
Set	*1*	*2*	*3*	*4*	*1*	*2*	*3*	*4*	*1*	*2*	*3*	*4*
$(dA)_n\cdot(dT)_n\cdot(dT')_n$												
dA	27	27	27	32	15	−20	4	1	23	18	27	32
dT	27	33	47	36	5	11	23	13	27	31	42	34
dT′	2	22	42	19	−2	−4	39	8	0	22	−16	17
$(rA)_n\cdot(rU)_n\cdot(rU')_n$												
rA	35	24	26	37	16	4	−3	9	31	24	26	36
rU	14	32	74	31	−3	−29	52	−15	14	−14	63	27
rU′	44	34	30	27	25	19	1	−8	37	29	30	26

a) α is the angles between the helix axis and the normal to the plane of an individual base.

fore, not only the value of $(\Delta\varepsilon/\varepsilon)_s$ at a fixed wavelength, but also the whole ELD spectrum inside the absorption region, should be measured to clarify the effect of the ionic strength on the helix structure. In contrast, the ELD spectrum of $(rA)_n\cdot(rU)_n\cdot(rU')_n$ is constant under all solution conditions, and the helix structure appears to be independent of M_w and I_s (Fig. 5b).

The ELD spectra of $(dA)_n\cdot(dT)_n\cdot(dT')_n$ are more undulatory than those of $(rA)_n\cdot(rU)_n\cdot(rU')_n$; $(\Delta\varepsilon/\varepsilon)_s$ values are different in the 190—210, 230—240, and 250—290 nm re-

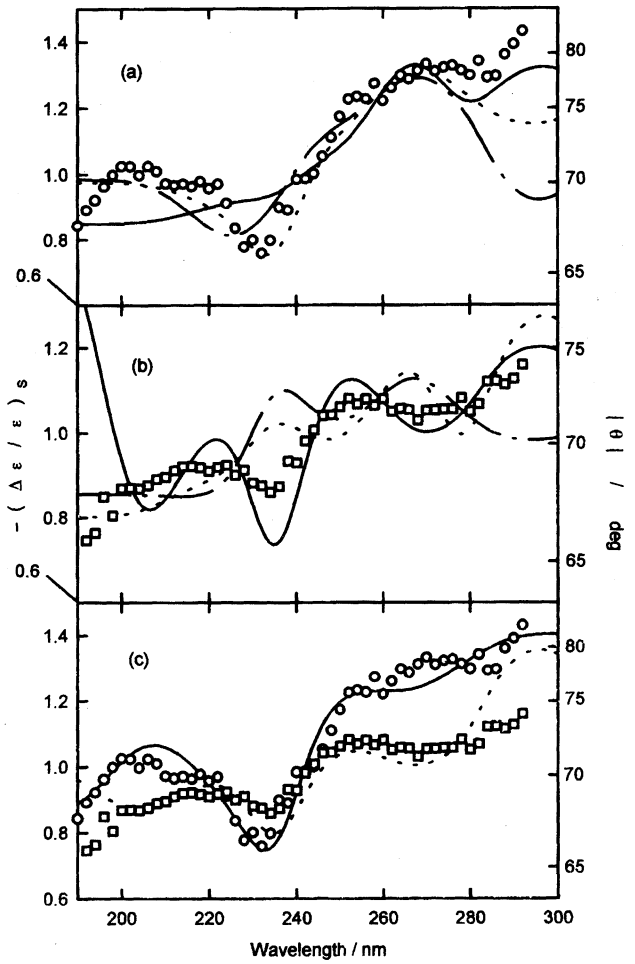

Fig. 7. Results of the analysis of measured ELD spectra of $(dA)_n\cdot(dT)_n\cdot(dT')_n$ (F2 at $I_s=0.0004$) (a) and $(rA)_n\cdot(rU)_n\cdot(rU')_n$ (F3 at $I_s=0.0004$) (b). Symbols are the experimental ELD spectra. Lines are the reproduced ELD spectra fitted to the experimental data with angles θ_R and θ_T, estimated with three sets of ξ: set *1* (—); set *2* (····); and set *3*, (- - -). The reproduced ELD spectra, best-fitted to the experimental spectra with set *4*, are shown in (c) for $(dA)_n\cdot(dT)_n\cdot(dT')_n$ (○,—) and for $(rA)_n\cdot(rU)_n\cdot(rU')_n$ (□, - - -).

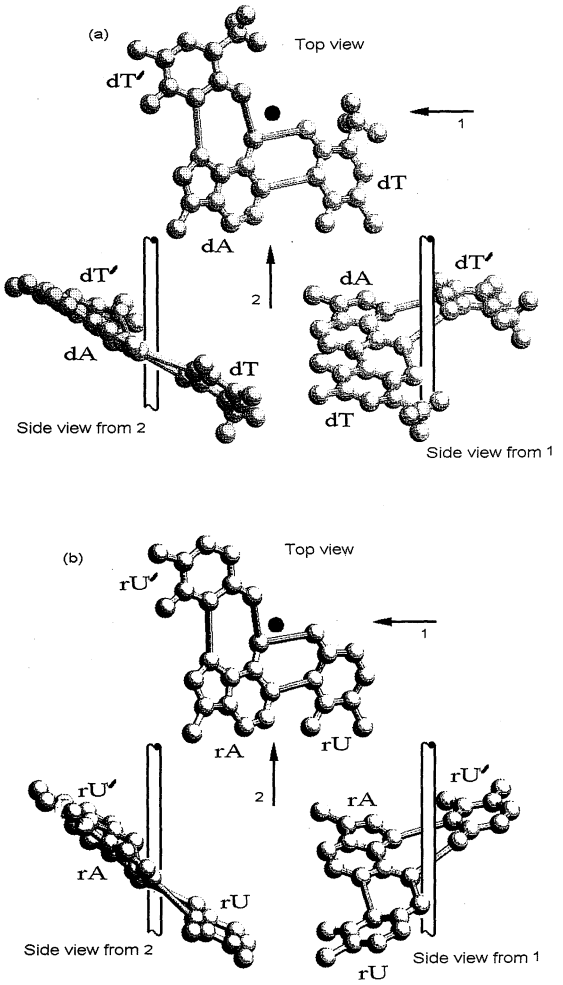

Fig. 8. Structural models proposed for dA·dT·dT′ (a) and rA·rU·rU′ (b) base-triples. These base-triples were rolled and titled by angles θ_R and θ_T, evaluated from the analysis of ELD spectra with ξ in set *4*. Base-triples are viewed down the helix axis (top), along the direction of arrows (1 and 2) orthogonal to the helix axis, which is denoted by closed circles and cylinders.

gions. Thus, their helical conformations are not identical to each other, probably because of the chemical difference in the constituent base and sugar. Even if the arrangements of the constituent bases in base-triples, dA·dT·dT′ and rA·rU·rU′, relative to the helix axis are identical with each other, the ELD spectra of two triple helices may not always be superimposable. This is because the optical characteristics and the directions of the individual component bands of thymine are not identical with those of uracil (cf. Table 3 and Eq. 4). Therefore, the isotropic absorption spectrum must be decomposed to the individual component bands in order to compare the structure of the helix from the ELD spectrum.

Deconvolution of Isotropic Absorption Spectra. Figure 6 shows the isotropic absorption spectrum and the decomposed component bands (lower), together with the second-derivative spectrum (upper) of $(dA)_n\cdot(dT)_n\cdot(dT')_n$ (a) and $(rA)_n\cdot(rU)_n\cdot(rU')_n$ (b). The isotropic spectrum of $(dA)_n\cdot(dT)_n\cdot(dT')_n$ could be decomposed to eight component bands, according to the procedure described in a previous paper.[21] The resultant isotropic and second-derivative spectra, calculated with these bands, are in good agreement with the experimental data (circles); thus, the deconvolution could be carried out successfully. Similarly to $(dA)_n\cdot(dT)_n\cdot(dT')_n$, the isotropic spectrum of $(rA)_n\cdot(rU)_n\cdot(rU')_n$ (circles in Fig. 6b) was decomposed to eight component bands. Each component band was assigned to the constituent base, as denoted by A (adenine), T (thymine), and U (uracil), by referring to the absorption spectra of the constituent mononucleotides and the optical characteristics of the component bands of bases in the literature.[32–37] Each component band assigned to pyrimidine base T or U was assumed to consist of two bands of equal magnitudes: one was assigned to the dT or rU base, which forms the Watson–Crick type base-pair with adenine base, and the other to dT′ or rU′ base, which

forms the Hoogsteen type base-pair with the adenine base (cf. Fig. 1a). Consequently, the total number of partial absorption bands was eleven for each triple helix. Furthermore, the transition moment direction of each component band was specified by angle ξ relative to the roll axis (cf. Fig. 1b). The values of ξ for A, T, or U reported in the literature are often contradictory, depending on the workers and their techniques of determination. In this work, four sets of ξ were selected and are given in Table 3, together with the optical characteristics and directions of the transition moments of the component absorption bands.

Simulation of ELD Spectra and Estimation of Angle ξ. The measured ELD spectra were simulated to evaluate the appropriate roll (θ_{Rk}) and tilt (θ_{Tk}) angles by substituting the ξ and $\varepsilon_{j,k}$ to Eq. 4 and by varying both θ_{Rk} and θ_{Tk} for each base (k=1—3) by means of nonlinear least-squares analysis.[21] The $\varepsilon_{j,k}$ value in Eq. 5 could be calculated from the optical parameters (λ_{max}, ε_{max}, δ) given in Table 3. Three sets (***1***—***3***) of ξ in Table 3 were chosen from previously reported values for their reliability test; set ***1*** from the single-crystal data,[32—34] set ***2*** from the film-dichroism data,[35,36] and set ***3*** from the data based on molecular orbital calculations.[37]

Figure 7 shows the experimental (symbols) and simulated (lines) ELD spectra of $(dA)_n\cdot(dT)_n\cdot(dT')_n$ (a) and $(rA)_n\cdot(rU)_n\cdot(rU')_n$ (b). The latter spectra were calculated to fit to the experimental data with appropriate paired values of θ_{Rk} and θ_{Tk}. For each triple helix, the ELD spectrum simulated with set ***2*** (dotted line) was best-fitted, though the fitting was barely satisfactory. In order to make the agreement between the experimental and simulated spectra better for $(dA)_n\cdot(dT)_n\cdot(dT')_n$ and $(rA)_n\cdot(rU)_n\cdot(rU')_n$, another set (set ***4***), in which the ξ values were expediently selected from sets ***1***—***3***, was used. The fitting was improved, but still far from being perfect (Fig. 7c). The ξ values given in Table 3 were determined for mononucleotide or isolated base. The directions of these transition moments are probably altered by hydrogen-bonds and stacking interaction between bases in a triple helix. Hence, the most critical reason for the discrepancy between calculated and experimental ELD spectra is due to the uncertainty of the reported ξ values in Table 3.[21] Precise determinations of the transition-moment directions of bases and the multiple base-pairs represent an important future subject for solving nucleic acid structures by the ELD method.

Evaluation of Roll Angle θ_R and Tilt Angle θ_T. The θ_R and θ_T values estimated by the ELD method are given in Table 4. It is clear from these angles that the bases constituting a base-triple, dA·dT·dT′ or rA·rU·rU′, do not lie on a common plane, but are inclined individually and differently with respect to the helix axis. The values of θ_R and θ_T of each base are sufficiently large. Therefore, two triple helices, $(dA)_n\cdot(dT)_n\cdot(dT')_n$ and $(rA)_n\cdot(rU)_n\cdot(rU')_n$, conclusively belong to the "A-family" helix structure, regarding the inclination of the bases to the helix axis, in spite of the still undetermined sugar conformation. The inclination angle (α) between the helix axis and the normal to a base plane is estimated from the corresponding set of θ_R and θ_T, as follows:[21—23]

$$\cos\alpha = |\cos\theta_R\cdot\cos\theta_T| . \quad (9)$$

A value of 28° for α, simply averaged for three bases and four sets of the dA·dT·dT′ base-triple in Table 4, is smaller than the corresponding value of 34° for the rA·rU·rU′ base-triple, indicating that the former is inclined with respect to the helix axis less than the latter, as an average.

As shown in Fig. 1a, the tilt axis (x) corresponds to the pseudodyad axis of the Watson–Crick type dA·dT or rA·rU pair, while the roll (y) axis corresponds to the pseudodyad axis of the Hoogsteen type dA·dT′ or rA·rU′ pair in dA·dT·dT′ or rA·rU·rU′ base-triple. Two additional angles ($\varkappa$ and θ_p) may now be introduced for a more detailed specification of the base-triple. The bent angle ($\varkappa$) is defined as [(θ_T of dA)−(θ_T of dT)] for the dA·dT pair and [(θ_T of rA)−(θ_T of rU)] for the rA·rU, whereas [(θ_R of dA)−(θ_R of dT′)] for the dA·dT′ pair and [(θ_R of rA)−(θ_R of rU′)] for the rA·rU′ pair.[44,45] The propeller-twist angle (θ_p) is defined as [(θ_R of dA)−(θ_R of dT)] for dA·dT and [(θ_R of rA)−(θ_R of rU)] for rA·rU, whereas [(θ_T of dT′)−(θ_T of dA)] for dA·dT′ and [(θ_T of rU′)−(θ_T of rA)] for rA·rU′.[44,45] The values of $\varkappa$ and θ_p were calculated with angles θ_R and θ_T for four sets (***1***—***4***) and are given in Table 5. Consequently, the dA·dT and dA·dT′ pairs, in the dA·dT·dT′ base-triple, and the rA·rU and rA·rU′ pairs in rA·rU·rU′ are all bent around the pseudodyad axes of these pairs and also propeller-twisted around the long axes, which correspond to the roll axis (y) for dA·dT and rA·rU, and the tilt axis (x) for dA·dT′ and rA·rU′. Evidently, the three angles (tilt θ_T, roll θ_R, and inclination α), evaluated with set ***3*** for theoretical ξ values, are less reasonable for bases dT, dT′, and rU, compared with the angles calculated from experimental sets ***1*** and ***2***. This unreasonableness indicates the difficult interpretation of the absorption spectra with the aid of a theoretical calculation. The θ_R and θ_T angles, simulated with ξ values in set ***4***, yield the most reasonable values among four sets, ***1***—***4***.

The base planes of $(dA)_n\cdot(dT)_n\cdot(dT')_n$ have been interpreted as being almost perpendicular to the helix axis on the basis of the structural determination by X-ray diffraction,[3,4] NMR,[5—9] and IR,[10] with which, however, the present ELD result is in disagreement. The discrepancy concerning the helix structures encountered with various techniques is partly due to the difference in the molecular weight of samples and the ionic solution conditions utilized in experiments. The ELD method is probably the only technique that enables the helix structure of high-molecular-weight nucleic acid to be determined in dilute aqueous ionic solutions, in which no interaction exists between solutes.

A Proposed Structure. Figure 8 shows plausible structure models for two base-triples, dA·dT·dT′ (a) and rA·rU·rU′ (b), proposed on the basis of θ_{Rk} and θ_{Tk} estimated with ξ values of set ***4*** (cf. Table 4). Both models were constructed from the ELD results in 0.1 mM $MgCl_2$–0.1 mM Tris/HCl solution (I_s=0.0004). For constructing these models, the lengths and angles of hydrogen bonds between bases were referred to the neutron[46] and X-ray[47] diffraction

Table 5. Bent, $\varkappa$, and Propeller-Twist, θ_p, Angles between Paired Bases in Degrees Calculated with Angles θ_R and θ_T for $(dA)_n\cdot(dT)_n\cdot(dT')_n$ and $(rA)_n\cdot(rU)_n\cdot(rU')_n$

Triplexes	$\varkappa$				θ_p			
paired bases	deg				deg			
Set	*1*	*2*	*3*	*4*	*1*	*2*	*3*	*4*
$(dA)_n\cdot(dT)_n\cdot(dT')_n$								
dA·dT	−4	−13	−15	−2	10	−31	−19	−12
dA·dT′	17	−16	−35	−7	−23	4	−43	−15
$(rA)_n\cdot(rU)_n\cdot(rU')_n$								
rA·rU	17	38	−37	9	19	33	−55	24
rA·rU′	−9	−15	−4	17	6	5	4	−10

Table 6. Hydrodynamic Properties of $(dA)_n\cdot(dT)_n\cdot(dT')_n$ and $(rA)_n\cdot(rU)_n\cdot(rU')_n$ with the Mg^{2+} Counterion

Triplexes	I_s	τ_w	L_w	h
fractions	10^{-3}	μs	Å	Å
$(dA)_n\cdot(dT)_n\cdot(dT')_n$				
F1	0.4	38.7	1120	3.0
	1.2	36.1	1090	2.9
F2	0.4	18.2	800	3.0
	1.2	18.5	800	3.0
F3	0.4	10.6	670	3.3
	1.2	9.4	640	3.2
$(rA)_n\cdot(rU)_n\cdot(rU')_n$				
F2	0.4	27.6	720	1.7
	1.2	27.3	720	1.7
F3	0.4	15.3	560	1.9
	1.2	15.4	560	1.9

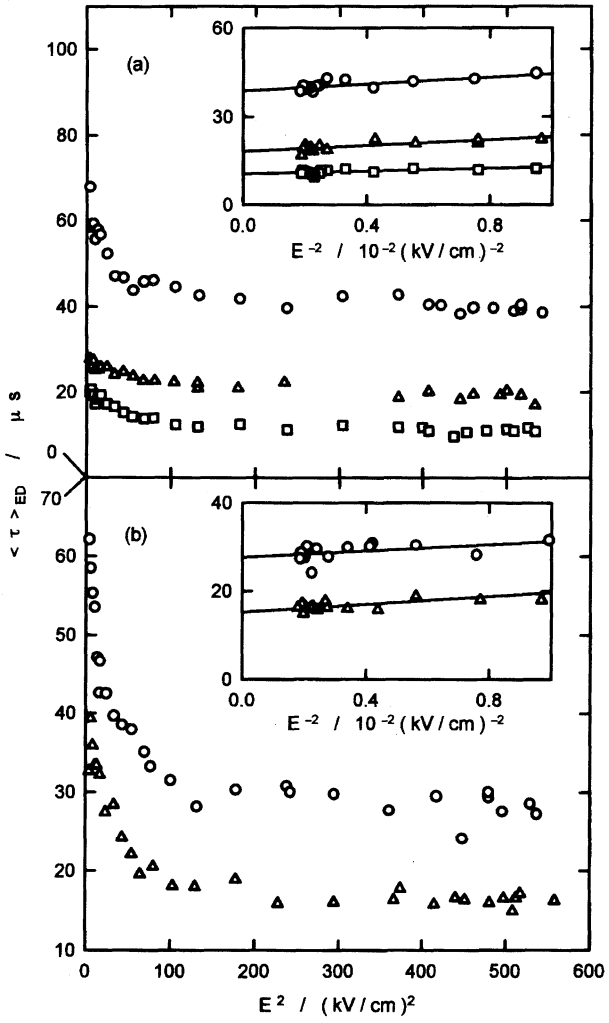

Fig. 9. Dependence of the rotational relaxation time, $\langle\tau\rangle_{ED}$, on electric field strength for $(dA)_n\cdot(dT)_n\cdot(dT')_n$ (a) and $(rA)_n\cdot(rU)_n\cdot(rU')_n$ (b). (a): F1 (○), F2 (△), and F3 (□) at I_s=0.0004. (b): F2 (○) and F3 (□) at I_s=0.0004. Inserts: $\langle\tau\rangle_{ED}$ vs. E^{-2} plots. Solid lines were drawn by the least-squares method.

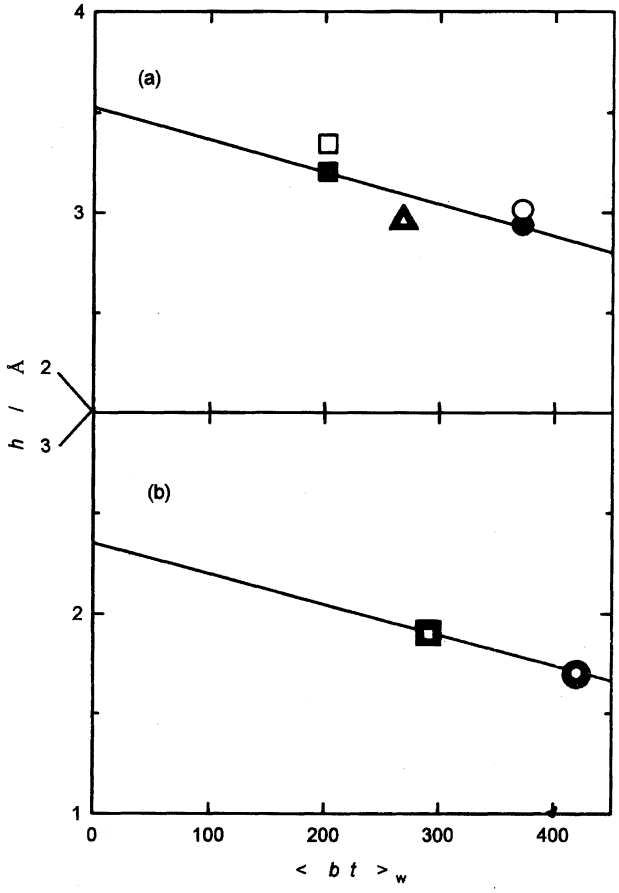

Fig. 10. Dependence of the axial translation per base-triple, h, on weight-average numbers of base-triple, $\langle bt\rangle_w$, for $(dA)_n\cdot(dT)_n\cdot(dT')_n$ (a) and $(rA)_n\cdot(rU)_n\cdot(rU')_n$ (b). (a): F1 (○), F2 (△), and F3 (□) at I_s=0.0004; F1 (●), F2 (▲), and F3 (■) at I=0.0012. (b): F2 (○) and F3 (□) at I_s=0.0004; F2 (●) and F3 (■) at I=0.0012. Solid lines were drawn by the least-squares method.

data. The base-triple is less inclined with respect to the helix axis for dA·dT·dT′ than for the rA·rU·rU′. A feature common to both base-triples is that the third base, dT′ or rU′, is inclined to the helix axis less than other two bases, dA and dT or rA and rU (cf. *side view from 2*). The relative arrangement of the Watson–Crick dA·dT pair in dA·dT·dT′ differs from that of the rA·rU pair in rA·rU·rU′. The dT base is rolled with a positive θ_R angle (the clockwise rotation as viewed from the front to rear of the paper in *side view from 1* of Fig. 8a) relative to the dA base, whereas the rU base is rolled with a negative θ_R angle against the rA base in Fig. 8b. The difference in the relative configurations may be due not only to two different kinds of sugars, but also to the steric hindrance between the methyl groups of the thymine bases; the distance between the carbon atoms in the methyl groups of dT and dT′ bases, constituting a base-triple, is 8.3 Å in Fig. 8b. The structure of $(rA)_n\cdot(rU)_n\cdot(rU')_n$ determined by the ELD method is consistent with the inference from the CD spectrum, though this is apparently not the case for $(dA)_n\cdot(dT)_n\cdot(dT')_n$.

Dependence of Relaxation Time on Electric Field. Figure 9 shows the dependence of the electric dichroism-average relaxation time ($\langle\tau\rangle_{ED}$) on the electric field applied prior to pulse removal for $(dA)_n\cdot(dT)_n\cdot(dT')_n$ (a) and $(rA)_n\cdot(rU)_n\cdot(rU')_n$ (b). In all sample solutions, the values of $\langle\tau\rangle_{ED}$ decrease with increasing electric field, approaching a limiting value at high electric fields. This feature is common to a polydisperse polymer sample with different chain lengths. The values of $\langle\tau\rangle_{ED}$ are less dependent on the field strength for $(dA)_n\cdot(dT)_n\cdot(dT')_n$ than for $(rA)_n\cdot(rU)_n\cdot(rU')_n$ because of the smaller degree of polydispersity ($M_w/M_n \fallingdotseq 1.10$ vs. 1.50) or better fractionation,[22,23,42] as given in Table 1. The values of $\langle\tau\rangle_{ED}$ at high electric fields are larger for higher molecular weight samples for both $(dA)_n\cdot(dT)_n\cdot(dT')_n$ and $(rA)_n\cdot(rU)_n\cdot(rU')_n$. The weight-average rotational relaxation time (τ_w) can be evaluated, by extrapolating the $\langle\tau\rangle_{ED}$ values to infinitely high electric fields. For this purpose, the $\langle\tau\rangle_{ED}$ values in the medium-to-high field region are plotted against the reciprocal of the second power of field strength and extrapolated to the ordinate by the last-squares method (cf. Inserts in Fig. 9). The values of τ_w are given in Table 6.

Axial Length of Translation per Base-Triple. In order to evaluate the axial translation per base-triple (h) τ_w was simulated with an iterative nonlinear least-squares analysis by substituting an appropriate h value in Eq. 8. The weight fraction ($f_w(M)$) in Eq. 6 and the molecular weight (M) in Eq. 8, both determined by the GPC/LALLS method (cf. Fig. 2) independently of ELD measurements, were used to calculate τ_w with the aid of Eqs. 6 and 8. The weight-average length (L_w) of a triple helix was calculated by multiplying h and the weight-average numbers of the base-triple $\langle bt\rangle_w$ (cf. Table 1). The τ_w, L_w, and h values of a triple helix with a diameter of 26 Å assumed for the double-stranded helices,[22,23] are given in Table 6, in which these parameters with other diameters (20 and 30 Å) are not given, because the dependence of τ_w on the diameter of a long helical polymer is not appreciable and because the third strand of $(dT')_n$ or $(rU')_n$ can approach the basic double-stranded helix smoothly from the major groove without either expansion or contraction of the diameter. The values of h of $(dA)_n\cdot(dT)_n\cdot(dT')_n$ and $(rA)_n\cdot(rU)_n\cdot(rU')_n$ are independent of I_s, but increase with a decrease in the molecular weight for each fraction. This dependence is probably due to the flexibility of the helical backbone. The intramolecular relaxation, which may result from the molecular flexibility, is faster than the rotational relaxation of a whole molecule, but makes finite contributions to the overall relaxation. The τ_w value presently estimated from the ELD decay signal is smaller than the overall molecular rotational relaxation time; hence; the overall length may be underestimated.[48] Furthermore, the triple-helix backbone, straightened under an electric field, returns to the field-absent and bent state after removing the field; thus, the apparent length, which equals the end-to-end distance of the backbone, is shorter than the contour length for any high-molecular-weight samples.

As mentioned above, the decay time ($\langle\tau_{ED}\rangle$) generally yields the end-to-end distance rather than the contour length. The flexibility of a backbone, which is defined as the ratio of the contour length (L) to the persistence length (P), decreases with a shorter L; thus, the relaxation intensity of a component with a faster decay time should become small as the degree of polymerization decreases. The effect of the flexibility on the decay time could be neglected at the limiting short L. Furthermore, Hagerman and Zimm found that the rotational relaxation time of a flexible chain can be expressed by multiplying a correction factor to the Broersma equation;[49] the modified equation is consistent with the original Broersma equation (Eq. 7) at the limiting low values of L/P. In order to remove the effect of the flexibility of helix backbone on the chain length, the h value should, therefore, be extrapolated to zero base-triple. Figure 10 shows the dependence of h on the base-triple $\langle bt\rangle_w$ for two triple helices. The limiting h values to zero $\langle bt\rangle_w$ (h_0) were estimated to be 3.7 and 2.4 Å for $(dA)_n\cdot(dT)_n\cdot(dT')_n$ and $(rA)_n\cdot(rU)_n\cdot(rU')_n$, respectively, by the least-squares method with six or four points of h. The value of 3.7 Å for $(dA)_n\cdot(dT)_n\cdot(dT')_n$ is longer than the values of 3.03—3.37 Å[41] for the B-type double-stranded DNA and other polydeoxyribonucleotide helices. The methyl groups of two thymine bases in a base-triple dA·dT·dT′ probably require some extra space for the axial elongation, in good agreement with the model shown in Fig. 8a (*side view form 2*). On the contrary, the h_0 value of 2.4 Å for $(rA)_n\cdot(rU)_n\cdot(rU')_n$ is smaller than 2.59—3.29 Å[41] for the A-type double-stranded RNA and other polyribonucleotide helices. This result supports the notion that the third strand $(rU')_n$ can easily "slip in" the major groove of the original duplex $(rA)_n\cdot(rU)_n$ without a steric hindrance to form the triplex (cf. model in Fig. 8b).

Conclusion

In the present study, the arrangement of bases and also the base-triple relative to the helix axis was determined for $(dA)_n\cdot(dT)_n\cdot(dT')_n$ and $(rA)_n\cdot(rU)_n\cdot(rU')_n$ from a detailed

analysis of ELD spectra. The axial translation per base-triple (h_0) of both triple helices was estimated from the weight-average rotational relaxation time (τ_w). Structural models for triplexes in aqueous solution were proposed based on angles θ_R and θ_T and h_0. The helical structure remains unaltered by an applied external electric field (no electrochromism effect). From the estimated θ_R and θ_T angles, each base, constituting a base-triple, lies out of a common plane, all bases being inclined considerably with respect to the helix axis. These results indicate that both triple helixes belong to the A-form family. The solution structure is appreciably different from that in the solid and fibrous states, as determined in X-ray studies. The values of h_0 are 3.7 and 2.4 Å per base-triple for $(dA)_n\cdot(dT)_n\cdot(dT')_n$ and $(rA)_n\cdot(rU)_n\cdot(rU')_n$, respectively. From a proposed structural model based on the θ_R and θ_T angles, which were estimated with set ***4*** of ξ, suggestions were made that the secondary structure of $(dA)_n\cdot(dT)_n\cdot(dT')_n$ is affected by the steric hindrance between methyl groups of thymine bases. In the present study, the angles for the direction of the transition moment (ξ) of nucleic acid bases or mononucleotides were taken from the published literature and used as such for analyzing the ELD spectra. The agreement between the experimental and simulated ELD spectra was inevitably less satisfactory. Therefore, accurate ξ values for hydrogen-bonded and/or stacking bases must be available for a more accurate structure determination by the ELD method. ELD techniques were demonstrated in the present work to be quite a versatile means for conformational studies of biologically important macromolecules.

This work was in part supported by Grants-in-Aid (K. Y.) for Scientific Research ((A) No. 02405008) and for Developmental Scientific Research ((B) No. 06554031) from the Ministry of Education, Science, Sports and Culture.

References

1) J. D. Watson and F. H. C. Crick, *Nature*, **171**, 737 (1953).
2) G. Felsenfeld, D. R. Davies, and A. Rich, *J. Am. Chem. Soc.*, **79**, 2023 (1957).
3) S. Arnott and P. J. Bond, *Nature New Biol.*, **244**, 99 (1973).
4) S. Arnott and E. Selsing, *J. Mol. Biol.*, **88**, 509 (1974).
5) P. Rajagopal and J. Feigon, *Biochemistry*, **28**, 7859 (1989).
6) D. S. Pilch, C. Levenson, and R. H. Shafer, *Proc. Natl. Acad. Sci. U.S.A.*, **87**, 1942 (1990).
7) K. Umemoto, M. H. Sarma, G. Gupta, J. Luo, and R. H. Sarma, *J. Am. Chem. Soc.*, **112**, 4539 (1990).
8) R. F. Macaya, P. Schultze, and J. Feigon, *J. Am. Chem. Soc.*, **114**, 781 (1992).
9) R. F. Macaya, E. Wang, P. Schultze, V. Sklenár, and J. Feigon, *J. Mol. Biol.*, **255**, 755 (1992).
10) F. B. Howard, H. T. Miles, K. Liu, J. Frazier, G. Raghunathan, and V. Sasisekharan, *Biochemistry*, **31**, 10671 (1992).
11) K. Yamaoka and E. Charney, *J. Am. Chem. Soc.*, **94**, 8963 (1972).
12) K. Yamaoka and E. Charney, *Macromolecules*, **6**, 66 (1973).
13) K. Yamaoka and K. Matsuda, *J. Sci. Hiroshima Univ., Ser. A*, **43**, 185 (1980).
14) K. Yamaoka and K. Matsuda, *Macromolecules*, **14**, 595 (1981).
15) E. Charney and K. Yamaoka, *Biochemistry*, **21**, 834 (1982).
16) K. Matsuda and K. Yamaoka, *Bull. Chem. Soc. Jpn.*, **55**, 1727 (1982).
17) K. Matsuda, *J. Sci. Hiroshima Univ., Ser. A*, **47**, 41 (1983).
18) K. Yamaoka, M. Asato, K. Matsuda, and K. Ueda, *Bull. Chem. Soc. Jpn.*, **57**, 1771 (1984).
19) K. Yamaoka, K. Ueda, and M. Asato, *J. Am. Chem. Soc.*, **106**, 3865 (1984).
20) K. Yamaoka, K. Ueda, and I. Kosako, *J. Am. Chem. Soc.*, **108**, 4619 (1986).
21) N. Ojima, K. Fukudome, and K. Yamaoka, *J. Sci. Hiroshima Univ., Ser. A*, **59**, 119 (1995).
22) K. Yamaoka, N. Ojima, and Y. Fujita, *J. Phys. Chem. B*, **101**, 1419 (1997).
23) K. Yamaoka, Y. Yamamoto, Y. Fujita, and N. Ojima, *J. Phys. Chem. B*, **101**, 837 (1997).
24) K. Yamaoka, M. Kimura, and M. Okada, *Bull. Chem. Soc. Jpn.*, **65**, 129 (1992).
25) M. Tanigawa, K. Fukudome, and K. Yamaoka, *J. Sci. Hiroshima Univ., Ser. A*, **58**, 123 (1994).
26) N. Ojima, K. Fukudome, and K. Yamaoka, *Polym. J.*, **26**, 303 (1994).
27) M. Tanigawa, M. Suzuto, K. Fukudome, and K. Yamaoka, *Macromolecules*, **29**, 7418 (1996).
28) M. Tanigawa, N. Mukaiyama, S. Shimokubo, K. Wakabayashi, Y. Fujita, K. Fukudome, and K. Yamaoka, *Polym. J.*, **26**, 291 (1994).
29) K. Fukudome, Y. Kumamoto, and K. Yamaoka, *Polym. J.*, **27**, 101 (1995).
30) C. H. Lee and E. Charney, *J. Mol. Biol.*, **161**, 289 (1982).
31) Y. Matsuoka and B. Nordén, *Biopolymers*, **21**, 2433 (1982).
32) T. P. Lewis and W. A. Eaton, *J. Am. Chem. Soc.*, **93**, 2054 (1971).
33) H. H. Chen and L. B. Clark, *J. Chem. Phys.*, **58**, 2593 (1973).
34) J. S. Novros and L. B. Clark, *J. Phys. Chem.*, **90**, 5666 (1986).
35) A. F. Fucaloro and L. S. Forster, *J. Am. Chem. Soc.*, **93**, 6433 (1971).
36) Y. Matsuoka and B. Nordén, *J. Phys. Chem.*, **86**, 1378 (1982).
37) W. Hug and I. Tinoco, Jr., *J. Am. Chem. Soc.*, **95**, 2803 (1973).
38) L. M. Schwartz, *Anal. Chem.*, **43**, 1336 (1971).
39) S. Broersma, *J. Chem. Phys.*, **32**, 1626 (1960).
40) S. L. Broitman, D. D. Im, and J. R. Fresco, *Proc. Natl. Acad. Sci. U.S.A.*, **84**, 5210 (1987).
41) W. Saenger, "Principles of Nucleic Acid Structure," Springer-Verlag, New York (1984).
42) M. Tanigawa and K. Yamaoka, *Bull. Chem. Soc. Jpn.*, **68**, 481 (1995).
43) D. Balasubramanian and E. Charney, *J. Phys. Chem.*, **85**, 1943 (1981).
44) IUPAC-IUB
Joint Commission on Biochemical Nomenclature, *J. Mol. Biol.*, **205**, 787 (1989).
45) J. M. Piriou, C. Ketterlé, L. Gabarro-Arpa, J. A. H. Cognet, and M. Le Bret, *Biophys. Chem.*, **50**, 323 (1994).
46) M. N. Frey, T. F. Koetzle, M. S. Lehmann, and W. C. Hamilton, *J. Chem. Phys.*, **59**, 915 (1973).
47) N. C. Seeman, J. M. Rosenberg, F. L. Suddath, J. J. P. Kim, and A. Rich, *J. Mol. Biol.*, **104**, 109 (1976).

48) K. Fukudome, *J. Chem. Phys.*, **102**, 9700 (1995).
49) P. J. Hagerman and B. H. Zimm, *Biopolymers*, **20**, 1481 (1981).